Journal of Rock Mechanics and Geotechnical Engineering 14 (2022) 448–459

Contents lists available at ScienceDirect

Journal of Rock Mechanics and Geotechnical Engineering

journal homepage: www.jrmge.cn

Full Length Article

Comparison of dominant frequency attenuation of blasting vibration for different charge structures

Pengchang Sun [a], Wenbo Lu [a,*], Junru Zhou [b], Xincheng Huang [a], Ming Chen [a], Qi Li [c]

[a] State Key Laboratory of Water Resources and Hydropower Engineering Science, Wuhan University, Wuhan, 430072, China
[b] School of Resource and Environmental Engineering, Wuhan University of Science and Technology, Wuhan, 430081, China
[c] Changjiang Institute of Survey, Planning, Design and Research, Wuhan, 430010, China

ARTICLE INFO

Article history:
Received 16 January 2021
Received in revised form
24 May 2021
Accepted 17 July 2021
Available online 20 August 2021

Keywords:
Dominant frequency
Blasting vibration
Attenuation law
Prediction equation
Charge structures

ABSTRACT

Dominant frequency attenuation is a significant concern for frequency-based criteria of blasting vibration control. It is necessary to develop a concise and practical prediction equation describing dominant frequency attenuation. In this paper, a prediction equation of dominant frequency that accounts for primary parameters influencing the dominant frequency was proposed based on theoretical and dimensional analyses. Three blasting experiments were carried out in the Chiwan parking lot for collecting blasting vibration data used to conduct regression analysis of the proposed prediction equation. The fitting equations were further adopted to compare the reliability of three different types of dominant frequencies in the proposed equation and to explore the effects of different charge structures on the dominant frequency attenuation. The apparent frequency proved to be more reliable to express the attenuation law of the dominant frequency. The reliability and superiority of the proposed equation employing the apparent frequency were verified by comparison with the other five prediction equations. The smaller blasthole diameter or decoupling ratio leads to the higher initial value and corresponding faster attenuation of the dominant frequency. The blasthole diameter has a greater influence on the dominant frequency attenuation than the decoupling ratio does. Among the charge structures applied in the experiments, the charge structure with decoupling ratio of 1.5 and blasthole diameter of 48 mm results in the greatest initial value and corresponding fastest attenuation of the dominant frequency.

1. Introduction

Drilling and blasting continues to be an essential method of rock excavation, which is widely used in many engineering fields for its efficiency and effectiveness, but it also brings some adverse effects that are unavoidable and cannot be completely eliminated (Singh et al., 2016; Gu et al., 2017; Ma et al., 2017; Sharafat et al., 2019; Bhagade et al., 2021). Among all the adverse effects, blasting vibration is found to be the major concern that many researchers keep following due to its influence on the surrounding structures, sensitive devices, and people in nearby environments (Kuzu and Guclu, 2009; Amnieh et al., 2010; Dogan et al., 2013; Hajihassani et al., 2015; Iwano et al., 2020; Yan et al., 2020). As an important characteristic of blasting vibration and a key parameter of blasting vibration safety criteria, the dominant frequency of blasting vibration has not received enough attention than it deserves. Therefore, more tremendous efforts should be paid to investigate the characteristics of the dominant frequency.

The qualitative conclusions about the effects of the physico-mechanical properties of the rock mass, the characteristics of the explosive, and the blasting design on the dominant frequency were drawn from several pieces of research. Zhang et al. (2020) noticed that the distribution of the dominant frequency band is high and wide in jointed rock masses. With the increase of the distance from the blasting source, the dominant frequency is attenuated (Alvarez-Vigil et al., 2012; Zhong et al., 2012; Zhou et al., 2016; Huang et al., 2019). The dominant frequency is inversely proportional to the charge weight (Alvarez-Vigil et al., 2012; Zhong et al., 2012; Yuan et al., 2017). Trivino et al. (2012) analyzed the effects of charge length on the average frequency in direct travelling modes of stress waves. Man et al. (2020) investigated the frequency spectrum characteristics for different

* Corresponding author.
E-mail address: wblu@whu.edu.cn (W. Lu).
Peer review under responsibility of Institute of Rock and Soil Mechanics, Chinese Academy of Sciences.

https://doi.org/10.1016/j.jrmge.2021.07.002

charge structures in underground blasting. The effects of other parameters such as relative elevation and delay time on the dominant frequency were also explored (Zhao et al., 2011; Li et al., 2017; Zhang et al., 2020). The above findings pave an effective way to extract the parameters influencing the dominant frequency. However, those researches associated with the dominant frequency are limited in qualitative analysis.

Several prediction equations were developed to help comprehend the characteristics of the dominant frequency quantitatively. The prediction equation of the dominant frequency was initially proposed by Sadovskij (Zhou et al., 2019), in which only the distance from the blasting source was considered:

$$f = \frac{1}{k\log_{10} r} \tag{1}$$

where f is the dominant frequency, k is the site-related coefficient, and r is the distance from the blasting source to the monitoring point.

An equation considering the shear wave velocity C_s and the charge weight Q was proposed by Jiao (1995):

$$f = k\frac{C_s^{7/5}}{Q^{1/3}}\left(\frac{Q^{1/3}}{r}\right)^{2/5} \tag{2}$$

Taking account of the effects of the peak particle velocity (PPV) V, Zhang and Yu (2005) established a prediction equation of the dominant frequency by dimensional analysis:

$$f = k\frac{V}{r}\left(\frac{Q^{1/3}}{r}\right)^{k_1} \tag{3}$$

where k_1 denotes the attenuation coefficient of blasting vibration.

Meng and Guo (2009) deduced a prediction equation of the dominant frequency in a viscoelastic medium:

$$f = \frac{1/r}{k_2\left(Q^{1/3}/r\right) + k_3 r} \tag{4}$$

where k_2 and k_3 are charge- and distance-related coefficients, respectively.

Based on the grey relational and dimensional analyses, Li et al. (2016) developed a prediction equation of the dominant frequency that includes the effects of the relative elevation:

$$f = k\frac{V^{k_4}}{Q^{1/3}}\left(\frac{Q^{1/3}}{r}\right)^{k_1}\left(\frac{Q^{1/3}}{H}\right)^{k_5} \tag{5}$$

where k_4 and k_5 are the wave velocity- and relative elevation-related coefficients.

The above equations were used to predict the attenuation laws of the dominant frequency and quantitatively illustrated the relationships between the dominant frequency and the commonly discussed parameters, such as the charge weight and distance from the blasting source. With the development of intelligent algorithms, many other prediction equations of the dominant frequency were proposed (Alvarez-Vigil et al., 2012; Derbal et al., 2020). However, those prediction equations resulting from intelligent algorithms involve too many variables and are complicated when applied in engineering practices.

It should be noted that a lack of theoretical basis may prove to be a challenge in applying those prediction equations. In addition, the charge structures have an essential influence on the dominant frequency, but the relationships between the dominant frequency and the charge structures with different decoupling ratios or blasthole diameters in open-pit blasting have not been reported. Therefore, it is necessary to develop a concise and practical prediction equation of the dominant frequency based on theoretical analysis, and further adopt the developed equation to explore the attenuation laws of the dominant frequency for different charge structures.

2. Prediction equation of dominant frequency

2.1. Definitions of dominant frequency

There are three principal means commonly used to estimate the dominant frequency of blasting vibration. Their corresponding results are known as the dominant frequency f_d matching the peak of Fourier amplitude spectrum shown in Fig. 1b, the average frequency $\bar{f}$ obtained by calculating the weighted mean of f_d through Eq. (6), and the apparent frequency f_a obtained through picking two nearest zero-point crossings on either side of the waveform peak shown in Fig. 1a, respectively.

$$\bar{f} = \frac{\sum f_i A(f_i)}{\sum A(f_i)} \tag{6}$$

where f_i represents the individual frequency in the Fourier amplitude spectrum, and $A(f_i)$ is the amplitude associated with each frequency f_i.

Among the three types of dominant frequencies, no single one is inherently superior, and they are all effectively used for engineering applications (Trivino et al., 2012; Zhou et al., 2016; Liu et al., 2019).

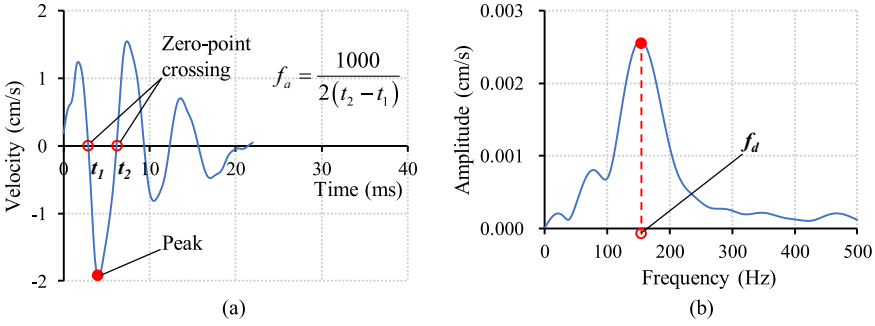

Fig. 1. Schematic diagram of definition for f_a and f_d: (a) Typical blasting vibration waveform, and (b) Fourier amplitude spectrum.

In a specific engineering application, the most suitable type of dominant frequency is proposed to be carefully selected by comparing their usefulness and applicability.

2.2. Main factors influencing dominant frequency

The inelastic zone, including the crushing and cracking zones around the blasthole, is regarded as an equivalent spherical charge.

The frequency spectrum of vibration due to practical blasting events can be then investigated by referring to the frequency spectrum of vibration due to blasting of a spherical charge, which is a widely accepted method (Kuzmenko et al., 1993; Zhou et al., 2016; Liu et al., 2019).

The theoretical solutions of the elastic waves triggered by a spherical charge in elastic media were yielded by Favreau (1969), and Kuzmenko et al. (1993) further deduced the frequency spectrum of vibration due to blasting of a spherical charge. The radial displacement u induced by a spherical charge can be represented by introducing potential function $\varphi(r,t)$ as

$$u = \frac{\partial \varphi(r,t)}{\partial r} \tag{7}$$

where r is the distance from the blasting source to the monitoring point, and t is the time.

At the boundary of the blasting source, the applied load is $p(t)$, then we have

$$\varphi(r,t) = \frac{r_e}{\rho\omega r}\int_0^s p(s-\tau)e^{-\eta\tau}\sin(\omega\tau)d\tau \tag{8}$$

where

$$s = t - \frac{r-r_e}{C_P},\ \eta = \frac{(1-2\nu)C_P}{(1-\nu)r_e},\ \omega = \frac{\sqrt{1-2\nu}C_P}{(1-\nu)r_e} \tag{9}$$

where ν is the Poisson's ratio, ρ is the density of rock, r_e is the radius of the equivalent cavity, and C_P is the longitudinal wave velocity.

Through the Fourier transformation, the complex spectrum of the displacement $S_d(j\omega)$ can be written as

$$S_d(j\omega) = S_p(j\omega)M(j\omega) \tag{10}$$

$$M(j\omega) = \frac{r_e\left[1/r^2 + j\omega/(rC_P)\right]}{4\mu/r_e^2 - (\lambda+2\mu)\omega^2/C_P^2 + 4\mu j\omega/(r_eC_P)} \tag{11}$$

where λ and μ are the elastic constants of Lame, and $S_p(j\omega)$ is the complex spectrum of the applied load $p(t)$.

From Eq. (10), the amplitude spectrum of the vibration velocity $F(\omega)$ is obtained as

$$F(\omega) = |jwS_d(j\omega)| = \frac{r_eC_P\omega\sqrt{C_P^2 + r^2\omega^2}|S_p(j\omega)| \Big/ (4\mu r^2)}{\sqrt{(C_P/r_e)^4 + [1-(\lambda+2\mu)/(2\mu)](C_P/r_e)^2\omega^2 + [(\lambda+2\mu)/(4\mu)]^2\omega^4}} \tag{12}$$

The law of variation of the applied load $p(t)$ is often used in the form as

$$p(t) = \begin{cases} 0 & (t < -t_u) \\ p_{max}(1+t/t_u) & (-t_u \le t < 0) \\ p_{max}(1-t/t_u) & (0 < t \le t_d) \\ 0 & (t > t_d) \end{cases} \tag{13}$$

where t_d is the reduction time and t_u is the build-up time of the applied load $p(t)$, respectively; and p_{max} is the maximum value of $p(t)$.

The amplitude spectrum of the applied load $p(t)$ becomes

$$S_p(\omega) = |S_p(j\omega)| = \frac{p_{max}}{a_eb_e\tau\omega^2}\sqrt{1 + a_e^2 + b_e^2 + 2a_eb_e\cos(\omega\tau) - 2[a_e\cos(b_e\omega\tau) + b_e\cos(a_e\omega\tau)]} \tag{14}$$

where $a_e = t_u/\tau$, $b_e = t_d/\tau$.

Based on an analysis of Eqs. (12) and (14), it follows that the amplitude spectrum of the vibration velocity $F(\omega)$ depends on the parameters of the blasting effects a_e, b_e, τ, the parameters of rock mass λ, μ, C_P, r_e, and the distance from the blasting source to the monitoring point r. The parameters of blasting effects are primarily determined by the charge weight Q, with the geometric parameters of blastholes being constant. The parameters of rock mass C_P and ρ can substitute for the elastic constants of Lame λ and μ. Therefore, the amplitude spectrum of the vibration velocity $F(\omega)$ primarily depends on the parameters Q, C_P, ρ, r_e and r.

2.3. Dimensional analysis of dominant frequency

According to the analysis in Section 2.2, the dominant frequency of blasting vibration is primarily determined by the parameters Q, C_P, ρ, r_e and r, and their units and dimensions are listed in Table 1.

The relationship between the dominant frequency and the five parameters listed in Table 1 was extracted by dimensional analysis. The parameters ρ, r_e and C_P, which cover the three base dimensions M, L and T, were chosen as independent variables. According to Buckingham π-theorem (Misic et al., 2010), the three independent dimensionless terms were developed as

Table 1
Primary parameters influencing dominant frequency and their dimensions.

Parameter	Symbol	Unit	Dimension
Charge weight per delay	Q	kg	M
Longitudinal wave velocity	C_P	m/s	LT^{-1}
Density of rock	ρ	kg/m^3	ML^{-3}
Radius of equivalent cavity	r_e	m	L
Distance from blasting source to monitoring point	r	m	L

$$\left.\begin{aligned}\pi_1 &= r_e^{\alpha_1}\rho^{\beta_1}C_P^{\gamma_1}f\\ \pi_2 &= r_e^{\alpha_2}\rho^{\beta_2}C_P^{\gamma_2}r\\ \pi_3 &= r_e^{\alpha_3}\rho^{\beta_3}C_P^{\gamma_3}Q\end{aligned}\right\} \tag{15}$$

After dimensionless computation, the three dimensionless terms can be written as

$$\pi_1 = \frac{fr_e}{C_P},\ \pi_2 = \frac{Q}{r_e^3\rho},\ \pi_3 = \frac{r}{r_e} \tag{16}$$

Then, the dominant frequency can be expressed as

$$\frac{fr_e}{C_P} = \Phi\left(\frac{Q}{r_e^3\rho}, \frac{r}{r_e}\right) \tag{17}$$

Thus, the relationship between the dominant frequency and the five parameters was extracted in the form as

$$f = \xi\frac{C_P}{r_e}\left(\frac{Q}{r_e^3\rho}\right)^{\xi_1}\left(\frac{r}{r_e}\right)^{\xi_2} \tag{18}$$

where ξ, ξ_1, and ξ_2 are the coefficients to be determined by the later regression analysis.

Under the condition of spherical charge, the charge weight Q is

$$Q = \frac{4}{3}\pi r_e^3\rho_e \tag{19}$$

where ρ_e is the density of the explosive.

After substituting Eq. (19) into Eq. (18), Eq. (18) can be simplified as

$$f = \frac{K}{Q^{1/3}}\left(\frac{Q^{1/3}}{r}\right)^{\alpha} \tag{20}$$

where K and α are the coefficients to be determined by the later regression analysis.

Furthermore, blasting seismic waves at intermediate or large distances from the blasting source in practical blasting events are more similar to cylindrical waves than spherical waves; hence Eq. (20) was revised to Eq. (21) based on the theory of cylindrical waves (Devine and Duvall, 1963).

$$f = \frac{K}{Q^{1/2}}\left(\frac{Q^{1/2}}{r}\right)^{\alpha} \tag{21}$$

3. Attenuation law of dominant frequency in blasting experiments

3.1. Site description and blasting design

As an important part of Shenzhen Metro Line #12 located in Shenzhen, Guangdong Province, China, the Chiwan parking lot shown in Fig. 2 was intended for parking metro vehicles. In order to bear the weight of the metro vehicles stopping in the parking lot,

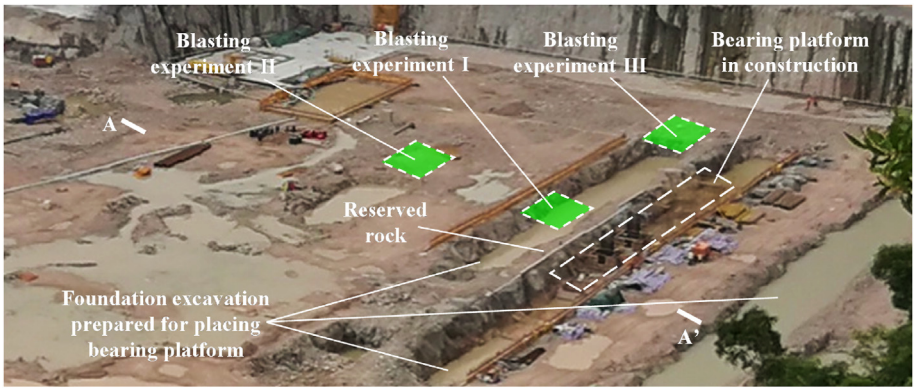

Fig. 2. Layout of Chiwan parking lot and blasting experiment sites.

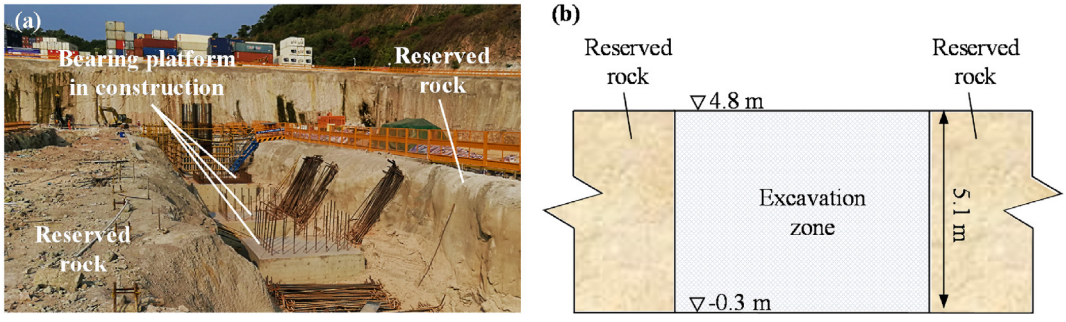

Fig. 3. Typical illustration of foundation excavation: (a) Photo showing bearing platform in construction, and (b) Schematic diagram of foundation excavation.

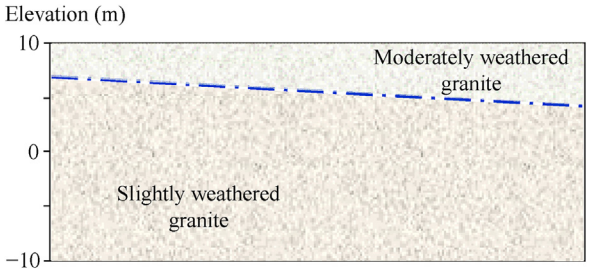

Fig. 4. Typical geological profile in the blasting experiment zone (*A-A′*).

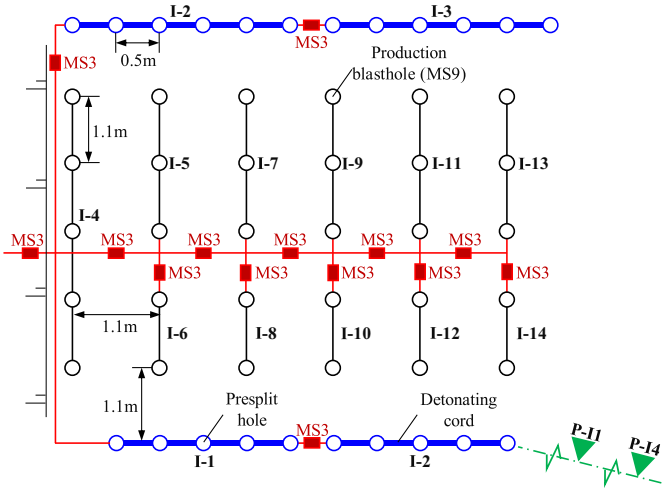

Fig. 5. Initiation network of blasting experiment I.

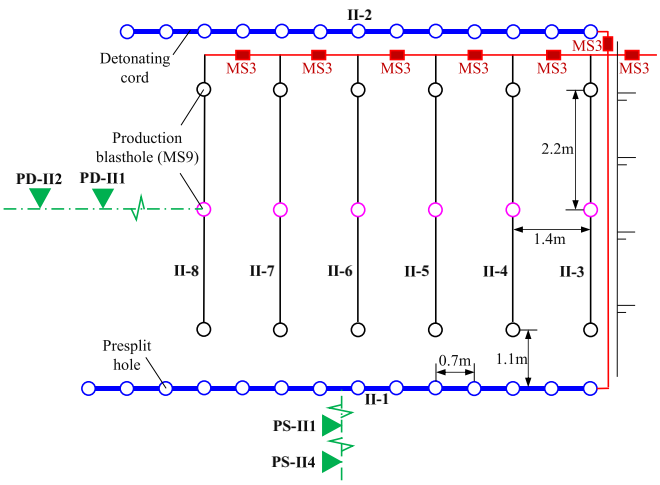

Fig. 6. Initiation network of blasting experiment II.

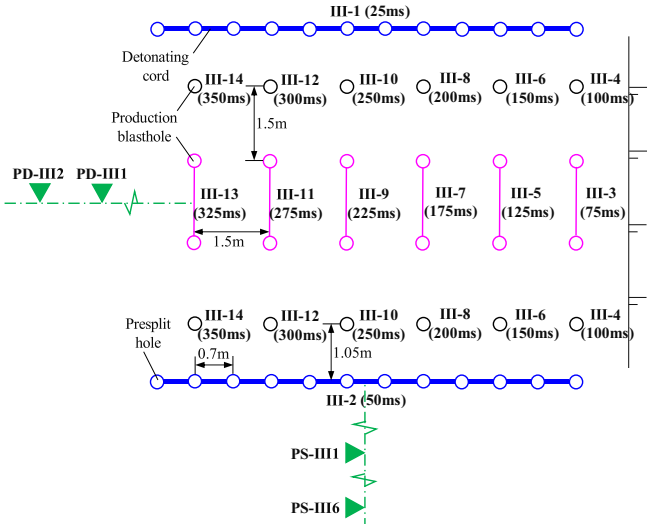

Fig. 7. Initiation network of blasting experiment III.

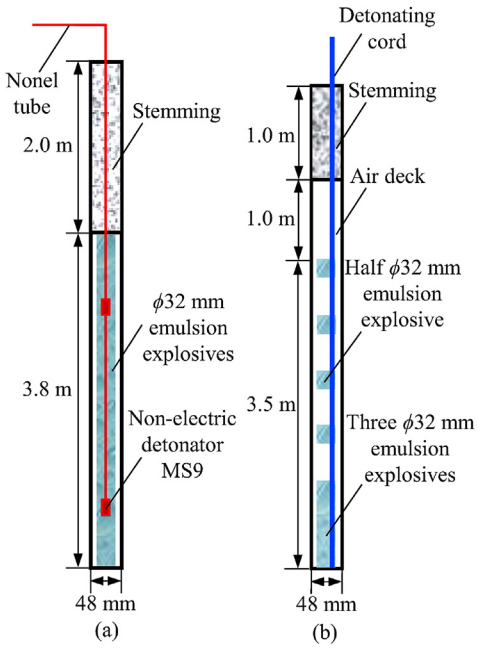

Fig. 8. Charge structures of blasting experiment I: (a) Production blastholes, and (b) Presplit holes.

the foundation of the parking lot was designed to be in the form of a large-scale reinforced concrete bearing platform in combination with coupling beams. The bearing platform is 5 m high, and its top surface is at an elevation of 4.8 m. The original ground surface of the parking lot has a topography around 4.8 m in elevation; hence large-scale trench excavation works for foundation construction need to be carried out in the parking lot by drilling and blasting method. The depth of the foundation excavation is 5.1 m, the upper part of which measuring 5 m high is prepared for placing the bearing platform, and the rest is prepared for paving cushion, as depicted in Fig. 3.

During the foundation construction, three blasting experiments were carried out for investigating the dominant frequency attenuation of blasting vibration using different charge structures, and they are blasting experiments I, II and III as marked in Fig. 2. As shown in Fig. 4, the rock mass in the experiment zone is mainly composed of slightly weathered coarse-grained granite whose quality is classified as grades II and III. The experiment zone provides a good foundation for exploring the effects of charge structures on the dominant frequency attenuation under approximately uniform lithologic and geological conditions.

The initiation networks of the blasting experiments I, II and III are displayed in Figs. 5–7, respectively. The blastholes in blasting

experiments I, II and III were composed of production blastholes and presplit holes. The production blastholes in blasting experiments I and II were fired by downhole non-electric detonators MS9, and those in blasting experiment III were fired by downhole electric detonators with different delay times. The presplit holes in the three blasting experiments were all instantly fired by detonating cords. Outside the production blastholes and presplit holes in blasting experiments I and II, non-electric detonators MS3 were used between delays.

According to the initiation networks displayed in Figs. 5–7, the firing sequences follow I-1 → I-2 → I-3 → I-4 → I-5 → I-6 → I-7 → I-8 → I-9 → I-10 → I-11 → I-12 → I-13 → I-14, II-1 → II-2 → II-3 → II-4 → II-5 → II-6 → II-7 → II-8, and III-1 → III-2 → III-3 → III-4 → III-5 → III-6 → III-7 → III-8 → III-9 → III-10 → III-11 → III-12 → III-13 → III-14 for the blasting experiments I, II and III, respectively.

The charge structures of blasting experiments I, II and III are displayed in Figs. 8–10, respectively. The radial decoupled charge was adopted for all blastholes, and the decoupling ratios R_d, defined as the ratio of the blasthole diameter d_b to the charge diameter d_c (Eq. (22)), for different types of blastholes in different blasting experiments are listed in Table 2. In the axial direction of the blastholes, continuous charge and air-spaced charge were adopted for production blastholes and presplit holes, respectively.

$$R_d = \frac{d_b}{d_c} \tag{22}$$

Besides the initiation networks and charge structures described above, the other detailed drilling and blasting parameters of the three blasting experiments are summarized in Table 2.

The vibrations induced by the three blasting experiments were collected by blasting vibration monitoring systems composed of intelligent monitors Blast-Cloud and triaxial velocity transducers shown in Fig. 11. The measurement ranges in velocity and frequency of the blasting vibration monitoring systems are 0.0005–35 cm/s and 5–500 Hz, respectively.

Defining the throwing direction of the blasting as the front, four monitoring systems P–I1 to P–I4 were arranged diagonally behind

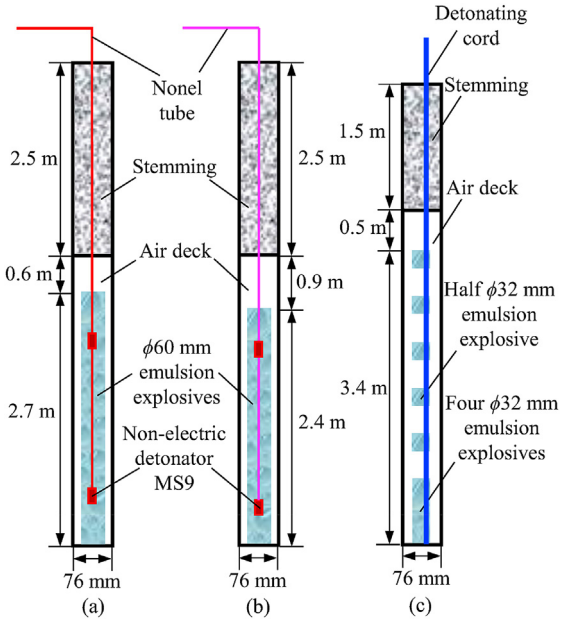

Fig. 9. Charge structures of blasting experiment II: (a) Production blastholes adjacent to presplit holes, (b) Middle production blastholes, and (c) Presplit holes.

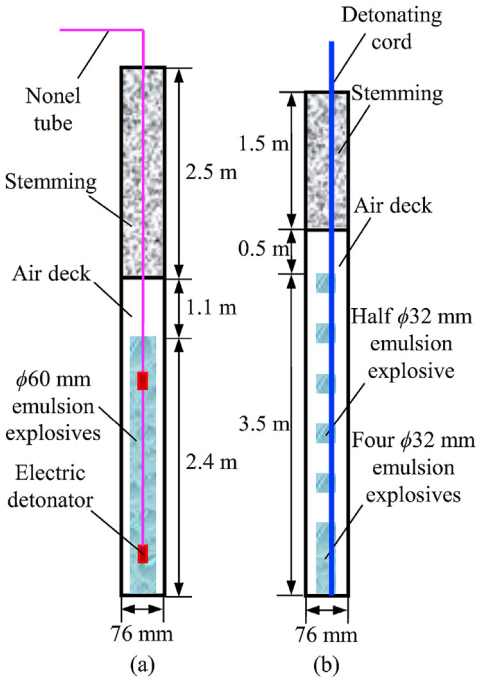

Fig. 10. Charge structures of blasting experiment III: (a) Production blastholes, and (b) Presplit holes.

Table 2
Detailed drilling and blasting parameters of three blasting experiments.

Parameter		Production blasthole			Presplit hole		
		I	II	III	I	II	III
Blasthole	Diameter (mm)	48	76	76	48	76	76
	Depth (m)	5.8	5.8	6	5.5	5.4	5.5
	Spacing (m)	1.1	2.2	1.5	0.5	0.7	0.7
	Burden (m)	1.1	1.4	1.5			
Charge	Diameter (mm)	32	60	60	32	32	32
	Stemming length (m)	2	2.5	2.5	1	1.5	1.5
	Weight per blasthole (kg)	3.8	8–9	8	1	1.95	1.95
	Decoupling ratio	1.5	1.27	1.27	1.5	2.38	2.38

the area of blasting experiment I, as shown in Figs. 5 and 12a. Two monitoring systems, PD-II1 and PD-II2, were arranged right behind the area of blasting experiment II, and four monitoring systems, PS-II1 to PS-II4, were arranged on the right side of the area of blasting experiment II, as shown in Figs. 6 and 12b. Two monitoring systems, PD-III1 and PD-III2, were arranged right behind the area of blasting experiment III, and six monitoring systems, PS-III1 to PS-III6, were arranged on the right side of the area of blasting experiment III, as shown in Figs. 7 and 12c.

3.2. Regression analysis of attenuation law

In order to obtain authentic attenuation laws of the dominant frequency, only direct seismic waves collected by blasting vibration monitoring systems were selected for regression analysis of the attenuation laws. Based on the initiation sequences of the three blasting experiments and specific layouts of blasting vibration monitoring points shown in Figs. 5–7 and 12, the recorded waveforms representing the direct waves were carefully selected and are listed in Table 3. The typical blasting vibration waveforms are displayed in Fig. 13.

Fig. 11. Blasting vibration monitoring system.

The selected blasting vibration waveforms listed in Table 3 were then divided into three groups according to their charge structures: (i) waveforms resulting from the presplit holes whose diameter d_b is 48 mm and R_d is 1.5, such as I-1, I-2 and I-3; (ii) waveforms resulting from the production blastholes whose diameter d_b is 76 mm and R_d is 1.27, such as III-3, III-5, III-7, III-9, III-11, III-13 and II-3 to II-8; and (iii) waveforms resulting from the presplit holes whose diameter d_b is 76 mm and R_d is 2.38, such as II-1, III-1 and III-2. Thus, the dominant frequency attenuation laws of blasting vibration using the three types of charge structures were investigated through regression analysis.

Linear least-squares method was adopted for regression analysis of the dominant frequency attenuation laws employing Eq. (21), and Pearson's correlation coefficient R was used for measuring the performance of the proposed equation. R is the covariance of the two variables (X, Y) divided by the product of their standard deviations, as given by

Table 3
Selected blasting vibration waveforms for regression analysis.

Blasting experiment	Monitoring point	Blasting vibration waveform
I	P–I1 to P–I4	I-1, I-2, I-3
II	PD-II1, PD-II2	II-3 to II-8
	PS-II1 to PS-II4	II-1
III	PD-III1, PD-III2	III-3, III-5, III-7, III-9, III-11, III-13
	PS-III1 to PS-III6	III-1, III-2

$$R = \frac{E[(X-\mu_X)(Y-\mu_Y)]}{\sigma_X \sigma_Y} \tag{23}$$

where E is the expectation, μ_X is the mean of X, μ_Y is the mean of Y, $\sigma_X = \sqrt{E(X^2) - [E(X)]^2}$ is the standard deviation of X, and $\sigma_Y = \sqrt{E(Y^2) - [E(Y)]^2}$ is the standard deviation of Y.

3.2.1. Case 1: $R_d = 1.5$ and $d_b = 48$ mm

The fitting results of the dominant frequency attenuation laws in Case 1 are presented in Fig. 14 and Table 4. The correlation coefficients above 0.77 were observed for all the fitting equations. Among the three types of dominant frequencies $\bar{f}$, f_a and f_d, the fitting equations of f_a have the highest values of the correlation coefficients, all of which are above 0.87, and those of f_d have the lowest values of the correlation coefficients. Therefore, it is more reliable to express the attenuation laws of the dominant frequency by using f_a than $\bar{f}$ and f_d. Furthermore, the attenuation of f_a with the increasing distance from the blasting source is the fastest while that

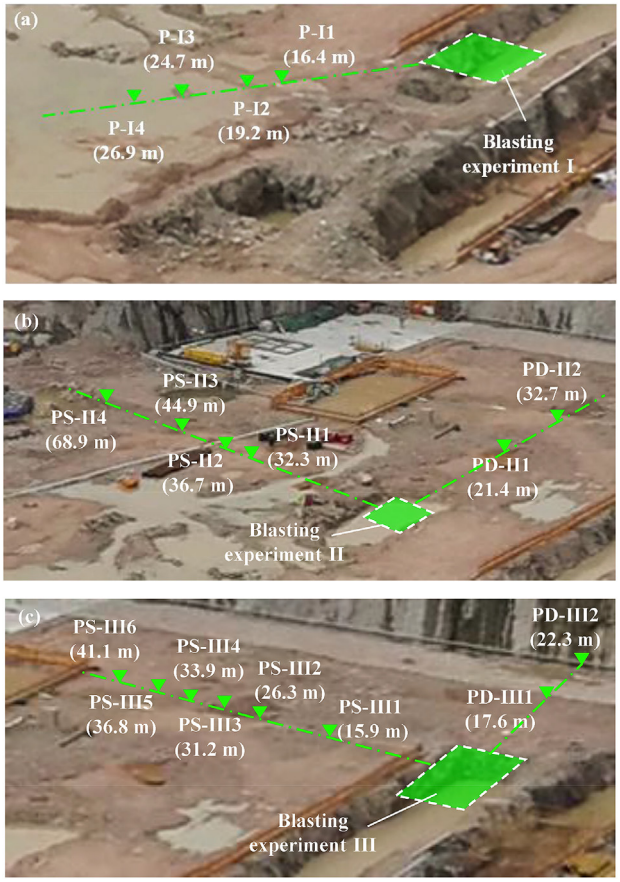

Fig. 12. Layout of blasting vibration monitoring system for blasting experiments (a) I, (b) II and (c) III.

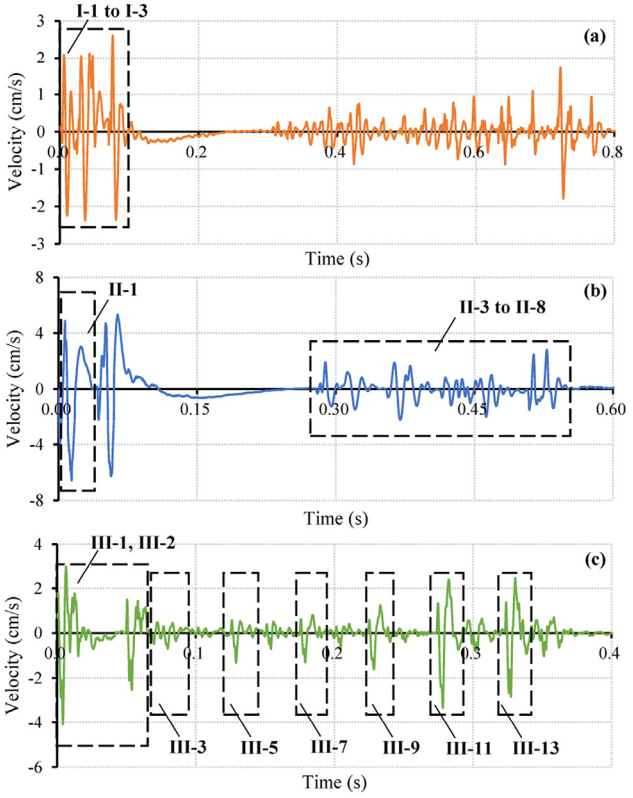

Fig. 13. Typical blasting vibration waveforms in vertical direction of (a) P–I1, (b) PD-II1, and (c) PD-III2.

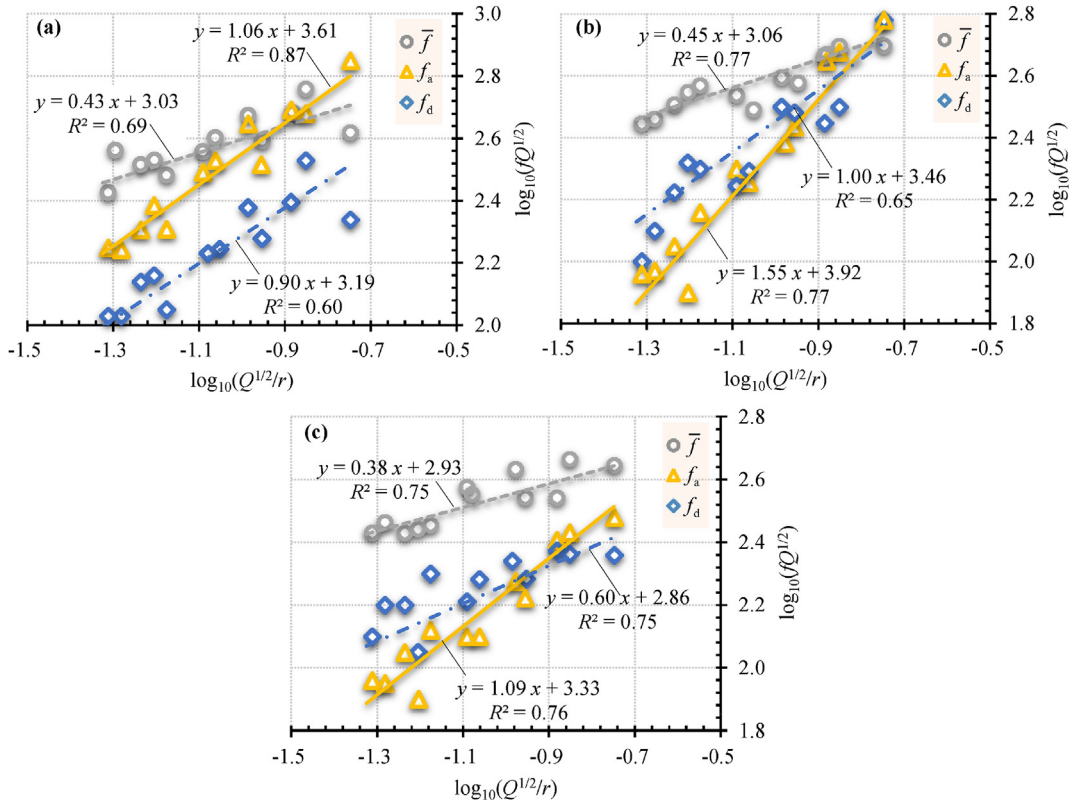

Fig. 14. Regression analysis of dominant frequency attenuation law for Case 1 ($R_d = 1.5$, $d_b = 48$ mm): (a) Longitudinal direction, (b) Transverse direction, and (c) Vertical direction.

Table 4
Attenuation laws of dominant frequency in Case 1 ($R_d = 1.5$, $d_b = 48$ mm).

Direction	Attenuation law of $\bar{f}$		Attenuation law of f_a		Attenuation law of f_d	
	Equation	R	Equation	R	Equation	R
Longitudinal	$\bar{f} = \frac{1067}{Q^{1/2}}\left(\frac{Q^{1/2}}{r}\right)^{0.43}$	0.828	$f_a = \frac{4059}{Q^{1/2}}\left(\frac{Q^{1/2}}{r}\right)^{1.06}$	0.932	$f_d = \frac{1541}{Q^{1/2}}\left(\frac{Q^{1/2}}{r}\right)^{0.9}$	0.774
Transverse	$\bar{f} = \frac{1148}{Q^{1/2}}\left(\frac{Q^{1/2}}{r}\right)^{0.45}$	0.875	$f_a = \frac{8285}{Q^{1/2}}\left(\frac{Q^{1/2}}{r}\right)^{1.55}$	0.876	$f_d = \frac{2857}{Q^{1/2}}\left(\frac{Q^{1/2}}{r}\right)^{1}$	0.808
Vertical	$\bar{f} = \frac{842}{Q^{1/2}}\left(\frac{Q^{1/2}}{r}\right)^{0.38}$	0.867	$f_a = \frac{2119}{Q^{1/2}}\left(\frac{Q^{1/2}}{r}\right)^{1.09}$	0.87	$f_d = \frac{732}{Q^{1/2}}\left(\frac{Q^{1/2}}{r}\right)^{0.6}$	0.865

of $\bar{f}$ is the slowest. Among the three directions, the dominant frequency of the transverse blasting vibration is fastest attenuated with the increasing distance.

3.2.2. Case 2: $R_d = 1.27$ and $d_b = 76$ mm

The fitting results of the dominant frequency attenuation laws in Case 2 are presented in Fig. 15 and Table 5. The correlation coefficients above 0.79 were observed for all the fitting equations. Among the three types of dominant frequencies $\bar{f}$, f_a and f_d, the fitting equations of f_a have the highest values of the correlation coefficients, all of which are above 0.85, and those of f_d have the lowest values. Therefore, it is more reliable to express the attenuation laws of the dominant frequency by using f_a than $\bar{f}$ and f_d. Furthermore, the attenuation of f_a with the increasing distance is the fastest, followed by f_d, while that of $\bar{f}$ is the slowest. Among the three directions, the dominant frequency of the transverse blasting vibration is fastest attenuated with the increasing distance.

3.2.3. Case 3: $R_d = 2.38$ and $d_b = 76$ mm

The fitting results of the dominant frequency attenuation laws in Case 3 are presented in Fig. 16 and Table 6. The correlation coefficients above 0.65 were observed for all the fitting equations. Among the three types of dominant frequencies $\bar{f}$, f_a and f_d, the fitting equations of f_a have the highest values of the correlation coefficients, all of which are above 0.81, and those of f_d have the lowest values. Therefore, it is more reliable to express the attenuation laws of the dominant frequency by using f_a than $\bar{f}$ and f_d. Furthermore, the attenuation of f_a with the increasing distance is the fastest, followed by f_d, while that of $\bar{f}$ is the slowest. Among the three directions, the dominant frequency of the transverse blasting vibration is fastest attenuated with the increasing distance.

4. Comparison with other prediction equations

In order to further demonstrate the reliability and applicability of the proposed Eq. (21), the other five equations, including Eqs.

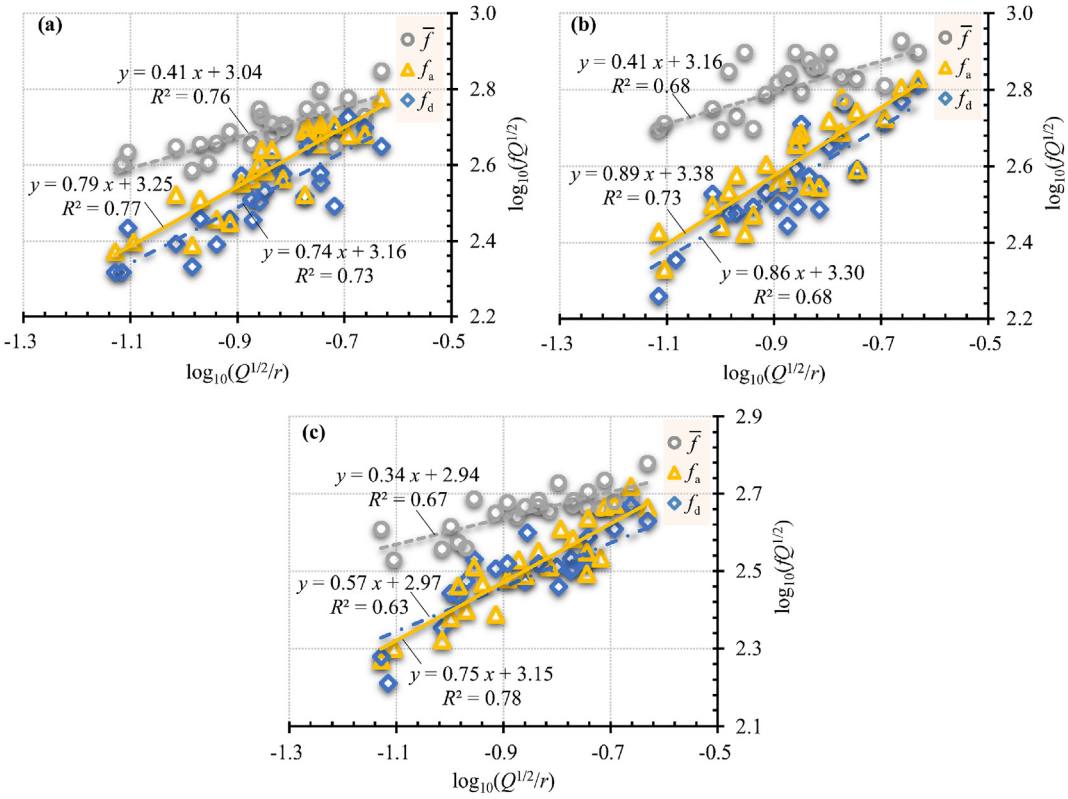

Fig. 15. Regression analysis of dominant frequency attenuation law for Case 2 (R_d = 1.27, d_b = 76 mm): (a) Longitudinal direction, (b) Transverse direction, and (c) Vertical direction.

Table 5
Attenuation laws of dominant frequency in case 2 (R_d = 1.27, d_b = 76 mm).

Direction	Attenuation law of $\bar{f}$		Attenuation law of f_a		Attenuation law of f_d	
	Equation	R	Equation	R	Equation	R
Longitudinal	$\bar{f} = \frac{1099}{Q^{1/2}}\left(\frac{Q^{1/2}}{r}\right)^{0.41}$	0.869	$f_a = \frac{1789}{Q^{1/2}}\left(\frac{Q^{1/2}}{r}\right)^{0.79}$	0.879	$f_d = \frac{1431}{Q^{1/2}}\left(\frac{Q^{1/2}}{r}\right)^{0.74}$	0.856
Transverse	$\bar{f} = \frac{1454}{Q^{1/2}}\left(\frac{Q^{1/2}}{r}\right)^{0.41}$	0.827	$f_a = \frac{2388}{Q^{1/2}}\left(\frac{Q^{1/2}}{r}\right)^{0.89}$	0.852	$f_d = \frac{2016}{Q^{1/2}}\left(\frac{Q^{1/2}}{r}\right)^{0.86}$	0.823
Vertical	$\bar{f} = \frac{874}{Q^{1/2}}\left(\frac{Q^{1/2}}{r}\right)^{0.34}$	0.816	$f_a = \frac{1414}{Q^{1/2}}\left(\frac{Q^{1/2}}{r}\right)^{0.75}$	0.884	$f_d = \frac{939}{Q^{1/2}}\left(\frac{Q^{1/2}}{r}\right)^{0.57}$	0.795

(1)–(5), were chosen for comparison. Due to the best reliability of the fitting equations employing the apparent frequency f_a among the three types of dominant frequencies, the regression analysis of the other five equations was conducted using the apparent frequency f_a, and the same collected data in the previous three cases were used. Complete results of the correlation coefficients of all the five equations (Eqs. (1)–(5)) as well as the proposed equation (Eq. (21)) in three cases are presented in Fig. 17.

As shown in Fig. 17, the correlation coefficients of the six equations vary enormously in the same case and direction; for example, the correlation coefficient of Eq. (2) in transverse direction for Case 1 is 0.08, which is far less than that of Eq. (21) with the value of 0.88 under the same condition. The correlation coefficients of the same equation in different cases or different directions also show a wide variation; for example, the correlation coefficient of Eq. (5) in the vertical direction for Case 1 is 0.89 while that for Case 2 is only 0.5.

All correlation coefficients of Eq. (21) are larger than 0.81, and its largest correlation coefficient reaches 0.93, which is superior to other prediction equations. There is no other equation whose correlation coefficients are all larger than 0.6 in all cases and directions. As a result, Eq. (21) has the best performance in predicting attenuation laws of the dominant frequency compared with the other five equations and can serve as a good predictor for dominant frequency attenuation of blasting vibration.

5. Discussions on dominant frequency attenuation for different charge structures

Since Eq. (21) proved to be reliable and superior in predicting the dominant frequency attenuation, further studies about comparison of the dominant frequency attenuation for different charge structures were conducted based on Eq. (21). The relationships of the dominant frequency f_a with both charge weight Q and the distance from the blasting source r with different charge structures are plotted in Fig. 18.

As shown in Fig. 18, the dominant frequency decays with the increasing distance under the constant charge weight in all cases.

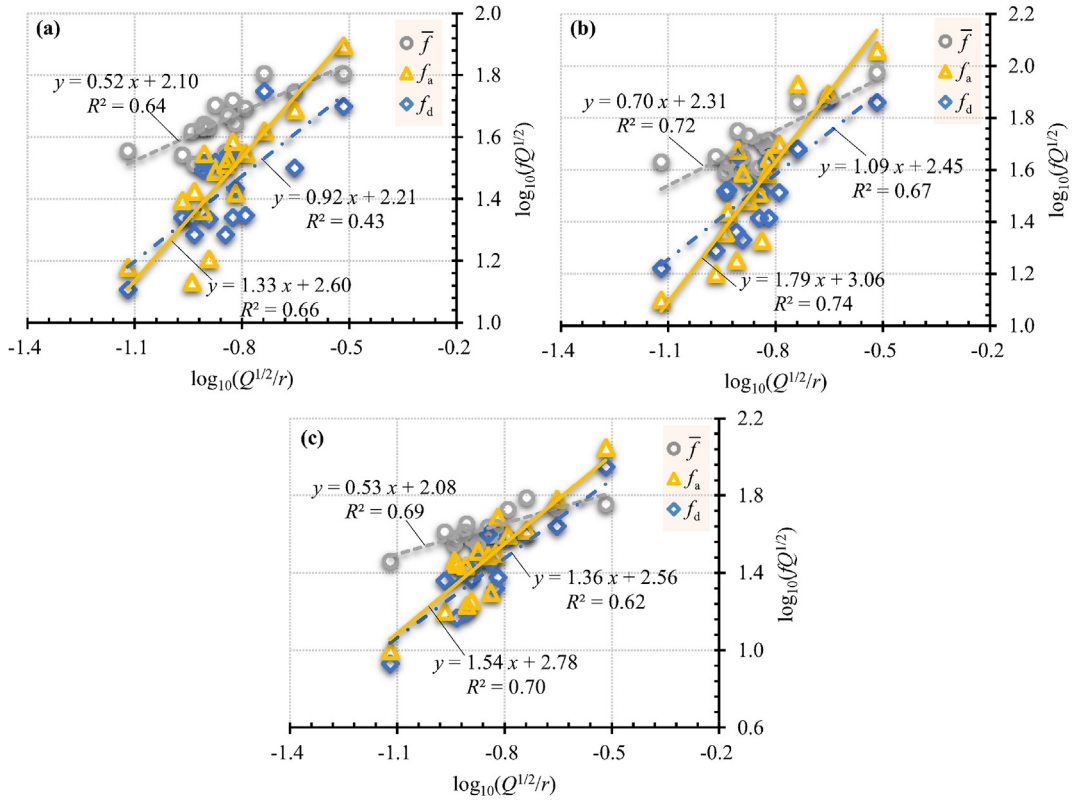

Fig. 16. Regression analysis of dominant frequency attenuation law for Case 3 ($R_d = 2.38$, $d_b = 76$ mm): (a) Longitudinal direction, (b) Transverse direction, and (c) Vertical direction.

Table 6
Attenuation laws of dominant frequency in Case 3 ($R_d = 2.38$, $d_b = 76$ mm).

Direction	Attenuation law of $\bar{f}$		Attenuation law of f_a		Attenuation law of f_d	
	Equation	R	Equation	R	Equation	R
Longitudinal	$\bar{f} = \frac{126}{Q^{1/2}}\left(\frac{Q^{1/2}}{r}\right)^{0.52}$	0.802	$f_a = \frac{395}{Q^{1/2}}\left(\frac{Q^{1/2}}{r}\right)^{1.33}$	0.814	$f_d = \frac{163}{Q^{1/2}}\left(\frac{Q^{1/2}}{r}\right)^{0.92}$	0.652
Transverse	$\bar{f} = \frac{202}{Q^{1/2}}\left(\frac{Q^{1/2}}{r}\right)^{0.7}$	0.85	$f_a = \frac{1157}{Q^{1/2}}\left(\frac{Q^{1/2}}{r}\right)^{1.79}$	0.86	$f_d = \frac{283}{Q^{1/2}}\left(\frac{Q^{1/2}}{r}\right)^{1.09}$	0.82
Vertical	$\bar{f} = \frac{120}{Q^{1/2}}\left(\frac{Q^{1/2}}{r}\right)^{0.53}$	0.832	$f_a = \frac{600}{Q^{1/2}}\left(\frac{Q^{1/2}}{r}\right)^{1.54}$	0.838	$f_d = \frac{365}{Q^{1/2}}\left(\frac{Q^{1/2}}{r}\right)^{1.36}$	0.785

As high-frequency blasting seismic waves decay more quickly than low-frequency ones do (Hustrulid, 1999), the decay level of the dominant frequency largely depends on the initial dominant frequency originating from the blasting source. Near the blasting source, the dominant frequencies in Case 1 are the largest with the values of over 150 Hz, and the dominant frequencies in Cases 2 and 3 are intermediate and the smallest with the values of 50–250 Hz and 0–100 Hz, respectively. Accordingly, the dominant frequency decays most quickly with the increase of the distance in Case 1, while the dominant frequency decays most slowly in Case 3. Similar results are observed for dominant frequencies in different directions. The initial dominant frequencies in the transverse direction are the largest, and those in the other two directions are smaller, which results from the strong movement confinement near the blasting source in the transverse direction but weaker confinement in the other two directions. Accordingly, the dominant frequency decays most quickly with the increasing distance in the transverse direction, while the dominant frequency decays more slowly in the other two directions, consistent with the results in Section 3.2.

Within the distance of 30–40 m, the dominant frequencies in the three cases decay rapidly. Beyond the distance of 40 m, the dominant frequencies in the three cases range from 0 Hz to 100 Hz, most of which are below 50 Hz, and they decay smoothly. Also, the influence of the charge weight on the dominant frequency attenuation within the distance of 30–40 m is greater than that beyond the distance of 40 m. In general, the influence of the charge weight on the dominant frequency is rather small compared with that of the distance from the blasting source.

According to the above analysis, the relationship of the dominant frequency attenuation with the distance for different charge structures is quite different, and it follows that the higher the initial dominant frequency is, the faster the dominant frequency decays within a certain distance. Within the distance of 30–40 m from the blasting source, the initial dominant frequency for the charge structure with $R_d = 1.5$ and $d_b = 48$ mm is the highest and thus the dominant frequency decays fastest, while the initial dominant frequency for the charge structure with $R_d = 2.38$ and $d_b = 76$ mm is the lowest and thus the dominant frequency decays most slowly. To sum up, the smaller blasthole diameter or decoupling ratio leads to

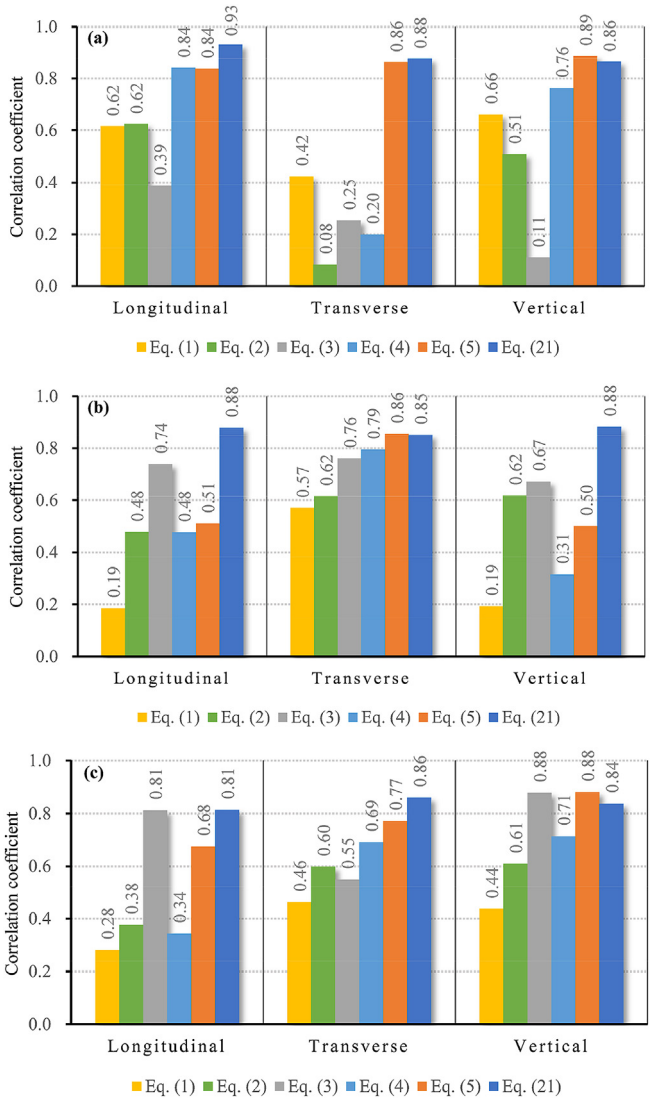

Fig. 17. Comparison of correlation coefficients of six equations in three cases: (a) Case 1 ($R_d = 1.5$, $d_b = 48$ mm); (b) Case 2 ($R_d = 1.27$, $d_b = 76$ mm); and (c) Case 3 ($R_d = 2.38$, $d_b = 76$ mm).

the higher initial dominant frequency and the corresponding faster attenuation of the dominant frequency. Also, the blasthole diameter has a more significant influence on the dominant frequency and its attenuation than the decoupling ratio does.

6. Conclusions

Through the theoretical and dimensional analyses, a prediction equation was proposed to predict the dominant frequency attenuation. Three blasting experiments in the Chiwan parking lot were then carried out to measure the reliability of the proposed equation. Based on the proposed equation, the applicability of the three types of dominant frequencies was compared, and the effects of charge structures on the dominant frequency attenuation were explored. Within the scope of this paper, the following conclusions can be drawn:

(1) The dominant frequency of blasting vibration is primarily determined by the charge weight, longitudinal wave velocity, rock density, equivalent cavity radius, and distance from the blasting source to the monitoring point. The proposed prediction equation of dominant frequency considering those parameters is in the form of Eq. (21).

(2) The apparent frequency f_a proved to be more reliable to express the attenuation laws of the dominant frequency. The reliability and superiority of the proposed equation using the apparent frequency f_a were verified by comparison with the other five prediction equations. The attenuation of f_a with the increasing distance from the blasting source is the fastest, while the attenuation of $\bar{f}$ is the slowest.

(3) The dominant frequency decays with the increasing distance, and the decay level is primarily based on the initial dominant frequency originating from the blasting source. Within a certain distance, the higher the initial dominant frequency is, the faster the dominant frequency decays. The influence of the charge weight on the dominant frequency attenuation is rather small compared with that of the distance from the blasting source.

(4) The dominant frequency attenuation mainly occurs within the distance of 30–40 m, and the dominant frequency decays smoothly beyond the distance of 40 m. The initial dominant frequency of the transverse blasting vibration is most prominent due to strong movement confinement, and the corresponding dominant frequency attenuation is the fastest.

(5) The smaller blasthole diameter or decoupling ratio leads to the higher initial dominant frequency and the faster attenuation of the dominant frequency, and the blasthole diameter has a more significant influence on the dominant frequency attenuation than the decoupling ratio does. Among the studied three types of charge structures, the initial dominant frequency for the charge structure with

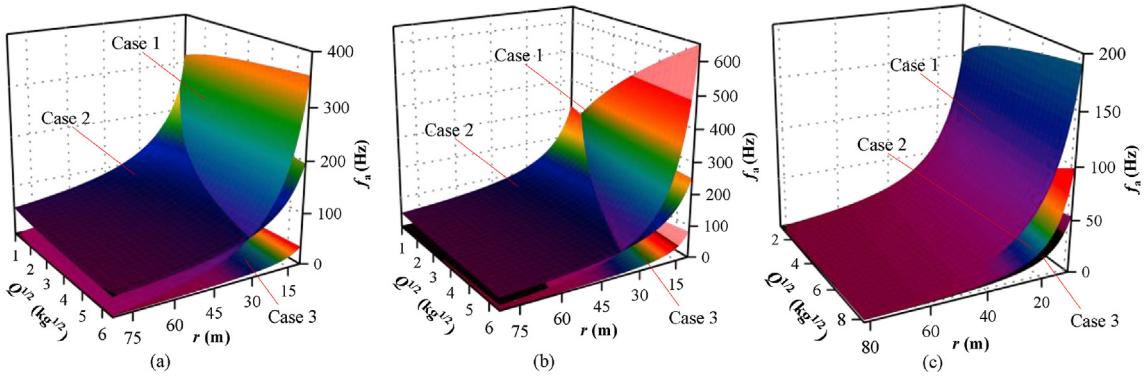

Fig. 18. Attenuation laws of dominant frequency for different charge structures: (a) Longitudinal direction, (b) Transverse direction, and (c) Vertical direction.

R_d = 1.5 and d_b = 48 mm is the highest, and the corresponding dominant frequency attenuation is the fastest.

It is important to note that only three cases of charge structures were included in this paper to investigate their effects on the dominant frequency attenuation, and it is necessary to carry out more blasting experiments for further study.

Declaration of competing interest

The authors declare that they have no known competing financial interests or personal relationships that could have appeared to influence the work reported in this paper.

Acknowledgments

This work was supported by National Natural Science Foundation of China (Grant Nos. 51779190 and 51909196) and Postdoctoral Science Foundation of China (Grant No. 2020T130569).

References

Alvarez-Vigil, A.E., Gonzalez-Nicieza, C., Gayarre, F.L., Alvarez-Fernandez, M.I., 2012. Predicting blasting propagation velocity and vibration frequency using artificial neural networks. Int. J. Rock Mech. Min. Sci. 55, 108–116.
Amnieh, H.B., Mozdianfard, M.R., Siamaki, A., 2010. Predicting of blasting vibrations in Sarcheshmeh copper mine by neural network. Saf. Sci. 48 (3), 319–325.
Bhagade, N.V., Murthy, V.M.S.R., Budi, G., 2021. Measurement and control of seismic effects in large scale dragline bench blasts - an approach. Measurement 168, 108390.
Derbal, I., Bourahla, N., Mebarki, A., Bahar, R., 2020. Neural network-based prediction of ground time history responses. Eur. J. Environ. Civ. Eng. 24 (1), 123–140.
Devine, J.P., Duvall, W.I., 1963. Effect of charge weight on vibration levels for millisecond delayed quarry blasts. Seismol Res. Lett. 34 (2), 16–24.
Dogan, O., Anil, O., Akbas, S.O., Kantar, E., Erdem, R.T., 2013. Evaluation of blast-induced ground vibration effects in a new residential zone. Soil Dynam. Earthq. Eng. 50, 168–181.
Favreau, R.F., 1969. Generation of strain waves in rock by an explosion in a spherical cavity. J. Geophys. Res. 74 (17), 4267–4280.
Gu, W.B., Wang, Z.X., Liu, J.Q., Xu, J.L., Liu, X., Cao, T., 2017. Water-depth-based prediction formula for the blasting vibration velocity of lighthouse caused by underwater drilling blasting. Shock Vib., 7340845, 2017.
Hajihassani, M., Armaghani, D.J., Marto, A., Mohamad, E.T., 2015. Ground vibration prediction in quarry blasting through an artificial neural network optimized by imperialist competitive algorithm. Bull. Eng. Geol. Environ. 74, 873–886.
Huang, D., Cui, S., Li, X.Q., 2019. Wavelet packet analysis of blasting vibration signal of mountain tunnel. Soil Dynam. Earthq. Eng. 117, 72–80.
Hustrulid, W., 1999. Blasting Principles for Open Pit Mining. A.A. Balkema, Rotterdam, the Netherlands.
Iwano, K., Hashiba, K., Nagae, J., Fukui, K., 2020. Reduction of tunnel blasting induced ground vibrations using advanced electronic detonators. Tunn. Undergr. Space Technol. 105, 103556.
Jiao, Y.B., 1995. Research on the standard of blasting seismic safety assessment. Blasting 12 (3), 45–47 (in Chinese).
Kuzmenko, A.A., Vorobev, V.D., Denisyuk, I.I., Dauetas, A.A., 1993. Seismic Effects of Blasting in Rock. Routledge, London, UK.
Kuzu, C., Guclu, E., 2009. The problem of human response to blast induced vibrations in tunnel construction and mitigation of vibration effects using cautious blasting in half-face blasting rounds. Tunn. Undergr. Space Technol. 24 (1), 53–61.
Li, H.B., Li, X.F., Li, J.C., Xia, X., Wang, X.W., 2016. Application of coupled analysis methods for prediction of blast-induced dominant vibration frequency. Earthq. Eng. Eng. Vib. 15, 153–162.
Li, P., Lu, W.B., Wu, X.X., Chen, M., Yan, P., Hu, Y.G., 2017. Spectral prediction and control of blast vibrations during the excavation of high dam abutment slopes with millisecond-delay blasting. Soil Dynam. Earthq. Eng. 94, 116–124.
Liu, D., Lu, W.B., Liu, Y.J., Chen, M., Yan, P., Sun, P.C., 2019. Analysis of the main factors influencing the dominant frequency of blast vibration. Shock Vib., 8480905, 2019.
Ma, H., Wang, H.L., He, C., Zhang, Z.Y., Ma, X., 2017. Influences of blasting sequence on the vibration velocity of surface particles: a case study of Qingdao metro, China. Geotech. Geol. Eng. 35, 485–492.
Man, K., Liu, X.L., Song, Z.F., 2020. Frequency spectrum and wavelet packet analyses of blasting vibration signals for different charge structures in blasting peripheral holes. Adv. Civ. Eng., 8897441, 2020.
Meng, H.L., Guo, F., 2009. Experimental research on the master frequency of blasting seismic wave. J. Railway Eng. Soc. 11 (11), 81–83 (in Chinese).
Misic, T., Najdanovic-Lukic, M., Nesic, L., 2010. Dimensional analysis in physics and the Buckingham theorem. Eur. J. Phys. 31, 893.
Sharafat, A., Tanoli, W.A., Raptis, G., Seo, J.W., 2019. Controlled blasting in underground construction: a case study of a tunnel plug demolition in the Neelum Jhelum hydroelectric project. Tunn. Undergr. Space Technol. 93, 103098.
Singh, P.K., Roy, M.P., Paswan, R.K., Sarim, M., Kumar, S., Jha, R.R., 2016. Rock fragmentation control in opencast blasting. J. Rock Mech. Geotech. Eng. 8 (2), 225–237.
Trivino, L.F., Mohanty, B., Milkereit, B., 2012. Seismic waveforms from explosive sources located in boreholes and initiated in different directions. J. Appl. Geophys. 87, 81–93.
Yan, Y., Hou, X.M., Fei, H.L., 2020. Review of predicting the blast-induced ground vibrations to reduce impacts on ambient urban communities. J. Clean. Prod. 260, 121135.
Yuan, P., Xu, Y., Zheng, Z.T., 2017. Time-frequency analyses of blasting vibration signals in single-hole blasting model experiments. J. Vibroeng. 19 (1), 363–375.
Zhang, L.G., Yu, Y.L., 2005. Research on the relationship of main vibration frequency of blasting vibration and peak particle velocity. Nonferrous Met. 57 (4), 32–34 (in Chinese).
Zhang, S.H., Gao, W.X., Yan, L., Liu, J.C., Liu, L.S., 2020. The characteristics of blasting vibration frequency bands in jointed rock mass slope. Environ. Earth Sci. 79, 519.
Zhao, M.S., Zhang, J.H., Yi, C.P., 2011. Time-frequency characteristics of blasting vibration signals measured in milliseconds. Min. Sci. Technol. 21 (3), 349–352.
Zhong, G.S., Ao, L.P., Zhao, K., 2012. Influence of explosion parameters on wavelet packet frequency band energy distribution of blast vibration. J. Cent. South Univ. 19 (9), 2674–2680.
Zhou, J.R., Lu, W.B., Yan, P., Chen, M., Wang, G.H., 2016. Frequency-dependent attenuation of blasting vibration waves. Rock Mech. Rock Eng. 49, 4061–4072.
Zhou, J.R., Lu, W.B., Zhong, D.W., Leng, Z.D., Wu, L., Yan, P., 2019. Prediction of frequency-dependent attenuation of blast-induced vibration in underground excavation. Eur. J. Environ. Civ. Eng. 2019 1620134.

Pengchang Sun obtained his BSc degree in Hydropower Engineering from Wuhan University, China, in 2016, and is currently a PhD candidate in hydraulic engineering at the same university. His research interests include geotechnical engineering and scientific problems related to engineering blasting. He focuses on investigating the dynamic response of high rock slope under blasting vibration.